ICAS-88-5.9.2

BASIC ANALYSIS OF THE FLOW FIELDS OF SLENDER DELTA WINGS USING THE EULER EQUATIONS

S. Scherr and A. Das

Deutsche Forschungs- und Versuchsanstalt für Luft- und Raumfahrt e.V. (DFVLR), Institut für Entwurfsaerodynamik
D-3300 Braunschweig, Fed. Rep. Germany

Abstract

The physics of delta wings moving in an inviscid medium is discussed. Numerical simulation of the flowfield around a closely coupled canard-delta wing configuration is performed for a range of angles of attack in subsonic and transonic free-stream conditions. These results are compared with calculations for the delta wing without canard to illustrate the influence of the canard on the flow. Subsequently the physics of the flowfields with vortical flux lines is analyzed in detail. The origin of total pressure losses inside the spiraling vortices and the onset of vortex breakdown at higher incidence are discussed.

1. Introduction

The flowfield of a delta wing moving in an inviscid medium is a prime candidate for modelling with the Euler equations, as a large part of the crossflow field is involved in producing spiraling flow around the wing which causes additional vortex lift. The rolled up vortices of delta wings have been the subject of intensive research for 30 years - with much effort having been put both into theoretical and experimental treatment of the problem.

The first theoretical treatments were made using simplified analytical methods [1] to [6], followed by numerical procedures based on linearized theories [7]. Numerical methods based on the full potential equation found thereafter some limited applications as cited in [8]. A large number of contributions have been made recently on this topic, some solving the Euler equations [9] to [13], and a few using the Navier-Stokes equations [14] to investigate secondary phenomena. A number of essential questions about physical aspects of such flowfields and their numerical modelling remain open and research effort is currently being put forth in the field.

For the validation of theoretical results concerning the flowfields and aerodynamic derivatives of delta wings a large number of experimental results from older sources [15] to [18] as well as from some recent tests at higher Mach numbers [19] to [23] is available.

In the present paper the numerical treatment of the flowfield of a delta wing with canard is described. The solution procedure used is a finite volume Euler solver with a cell vertex discretization scheme. These results are compared with calculations for the delta wing alone to obtain an understanding of the influence of the canard on the flow.

A second objective of this work is the analysis of essential physical phenomena in the spiraling vortical flow of the inviscid medium. Some basic considerations on bound and free vortices and their effect on total pressure loss are discussed. An analogy with electromagnetic field lines is presented to describe vortex bursting.

2. Governing Equations and Solution Scheme

The three-dimensional unsteady Euler equations for compressible, inviscid flows may be written in integral form as

$$\frac{\partial}{\partial t} \int_{\Omega} \vec{W} \, d\Omega + \int_{\partial\Omega} \bar{\bar{F}} \cdot \bar{n} \, ds = 0 \qquad (1)$$

for a region Ω with boundary $\partial\Omega$. $\vec{n}$ is the unit outward normal to $\partial\Omega$. In cartesian coordinates, the solution vector $\vec{W}$ and the tensor of flux density $\bar{\bar{F}}$ are given by

$$\vec{W} = \begin{vmatrix} \rho \\ \rho u \\ \rho v \\ \rho w \\ \rho E \end{vmatrix}, \qquad \bar{\bar{F}} = \begin{vmatrix} \rho\vec{q} \\ \rho u\vec{q} + p\vec{i}_x \\ \rho v\vec{q} + p\vec{i}_y \\ \rho w\vec{q} + p\vec{i}_z \\ \rho E\vec{q} + p\vec{q} \end{vmatrix} \qquad (2)$$

where $\vec{i}_x, \vec{i}_y, \vec{i}_z$ are the cartesian unit vectors and $\vec{q} = u\vec{i}_x + v\vec{i}_y + w\vec{i}_z$ is the vector velocity. This system of first-order partial differential equations in the five unknowns ρ, u, v, w, E is closed by the equation of state for a perfect gas,

$$p = \frac{1}{2}(\gamma - 1)\rho\,(E - |\vec{q}|^2) \qquad (3)$$

in which γ is the ratio of specific heats c_p/c_v.

The basic solution scheme is a finite-volume spatial discretization with a Runge-Kutta integration in time, as described by Jameson et al. [24,25]. This has been implemented in the DFVLR Euler code CEVCATS as a cell-vertex discretization [26,27], in which the solution vector $\vec{W}$ is evaluated at the vertices of the mesh cells, i.e. at the grid points, with a distribution formula for the cell fluxes as proposed by Hall [28]. Since the equations are discretized using a central difference scheme, artificial dissipation must be added in order to damp out high frequency oscillations. The inclusion of a blend of second and fourth differences as dissipative fluxes allows the convergence of the procedure to a smooth solution. As we are only interested in steady-state flow fields, the integration in time is used exclusively to advance the solution toward the steady state. To this end several convergence accelerating techniques are employed: successive grid refinement, local time stepping, enthalpy damping, and implicit residual averaging. The application of these techniques has been shown to produce a significant reduction in the number of iterations required to obtain a solution [29].

CEVCATS is a block-structured code, i.e. it allows the subdivision of the computational domain into several blocks. This may be necessary because of the grid topology, or because of limitations in storage capacity of the computer. Each block consists of a regular array of hexahedral cells. Boundary conditions are imposed on the faces of the blocks or on rectangular subfaces, i.e. patches of m by n cells. Four types of boundary conditions have been implemented: 1) symmetry across a constant coordinate plane, 2) far field, using characteristic variables, 3) solid body, at which no flux is allowed through the body, and 4) internal cut, which is a cut in the interior of the solution domain. An internal cut may be a cut between two blocks which have been separated for storage requirements, may represent a periodicity condition, or may be required in the transformation of the geometry of the solution domain into a set of regular blocks. The solid body condition requires the generation of a body-fitted mesh system.

The CEVCATS code has also been extended to allow handling of grid singularities. These may occur when one physical point is represented by multiple grid points as in a polar singularity, at which many grid lines radiate out from the polar axis, or when a single grid line branches into two lines, as happens when an H-cut comes to a solid surface. In the latter case, one point next to the branch point will also have to be handled specially because of the five-point operator used in computing the fourth-order dissipation. Each of the grid points involved in a singular point is updated identically. The convective flux is calculated by summing the flux balances for each of the mesh cells adjacent to the singular point. The dissipation is simply calculated as the average value of the dissipation in each of the grid points.

3. Grid Generation

The configuration modelled in this investigation is that used in the US/European Vortex Flow Experiment. This consists of a 65° swept sharp leading edge delta wing with a cropped tip (Figure 1). The canard is aligned with the wing centerline in the x-y plane and has a leading edge sweepback of 60° and a trailing edge sweepback of 35°. The canard also has a cropped tip. Both wing and canard have a symmetric cross-sectional profile. No fuselage was modelled in any of the calculations, and the cropped tips were somewhat rounded in all the grids.

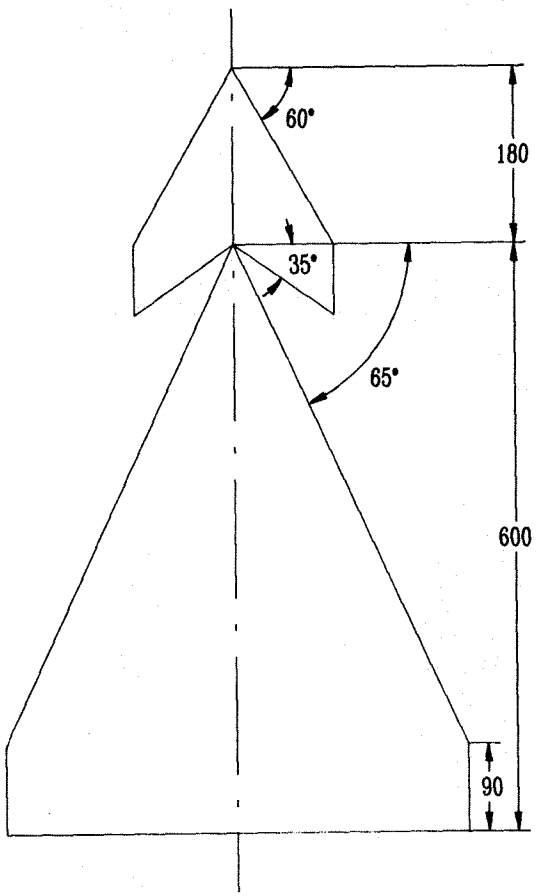

Fig. 1 Geometry of the VFE canard-delta configuration.

Previous calculations for the flow field over the wing alone have been performed in this institute on an O-O mesh [30]. This mesh has a size of 96x48x24 cells. The O-grid topology tends to give a better resolution at areas of interest in the solution domain when compared with an H-grid topology. When working with complicated geometries, however, it is often necessary or desirable to use H-grids. This proved to be the case for the integration of the canard into the grid. Other investigators [31] have modelled similar configurations with a canard farther forward of the wing inserted in a slit in an O-O-mesh, forming an H-H-mesh around the canard. In the present investigation, a purely H-H structure was used around both the wing and canard. This has the advantage of simplicity of construction and uniformity in handling of the wing and canard.

The present mesh is divided into two symmetric blocks, one for the upper region and one for the lower region of the flow field. The upper surface of the delta wing is discretized into 48x48 cells, with 24 cells in the direction normal to the wing. This is analogous to the O-O mesh. Furthermore, the canard is divided into 32x20 cells. Fifteen cells each lie upstream and downstream of the canard-wing combinations. Between the canard trailing edge and the wing leading edge are twenty cells. This creates a singularity at the wing apex, due to the close-coupling of the canard. The total mesh consists of 2 blocks with 118 cells in the streamwise direction, 72 cells in the spanwise direction, and 24 cells normal to the wing, for a total of 407,808 cells. The mesh was generated via tranfinite interpolation. A view of the mesh is shown in Figure 2.

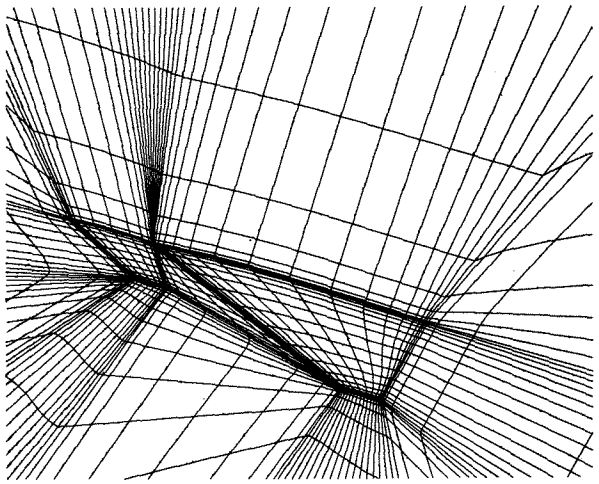

Fig. 2 Symmetry and water line planes of the mesh.

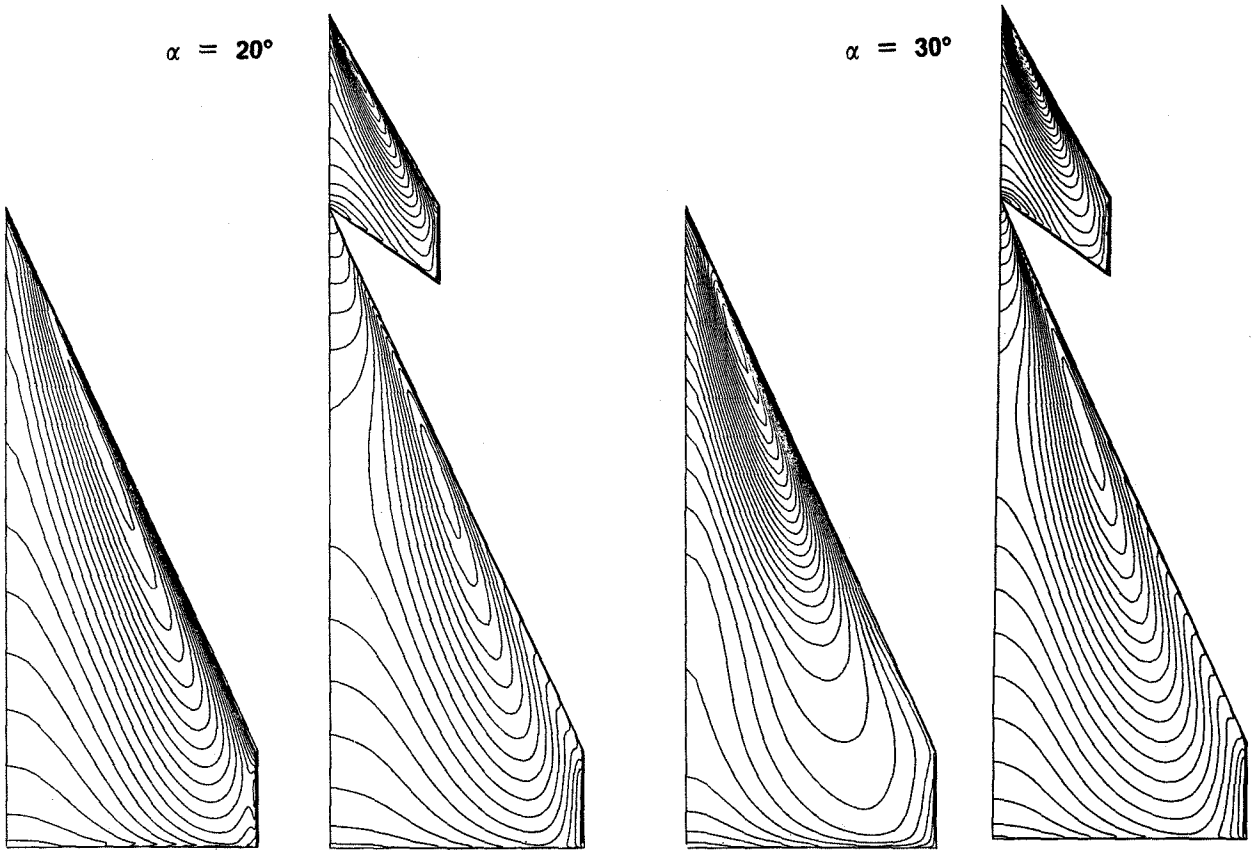

Fig. 3 Comparison of upper surface isobars, $M_\infty = 0.4$.

4. Numerical Results

The flow over the VFE canard-delta configuration has been computed for various angles of attack for Mach numbers of 0.4 and 0.85. A comparison of c_p distribution on the upper surface of the canard-delta configuration with that of the delta wing alone is shown in Figure 3 for two angles of attack at a Mach number of 0.4. For both configurations the low pressure region induced by the leading edge vortex moves up the leading edge toward the wing apex with increasing angle of attack. The influence of the canard vortex, however, causes this low pressure region to be shifted downstream. A consequence of this shift is that vortex bursting, which occurs over the wing at 30° angle of attack, is moved off the wing when the canard is present. Indeed, loss of lift due to vortex bursting is just beginning to be noticeable at α = 35° (Figure 4).

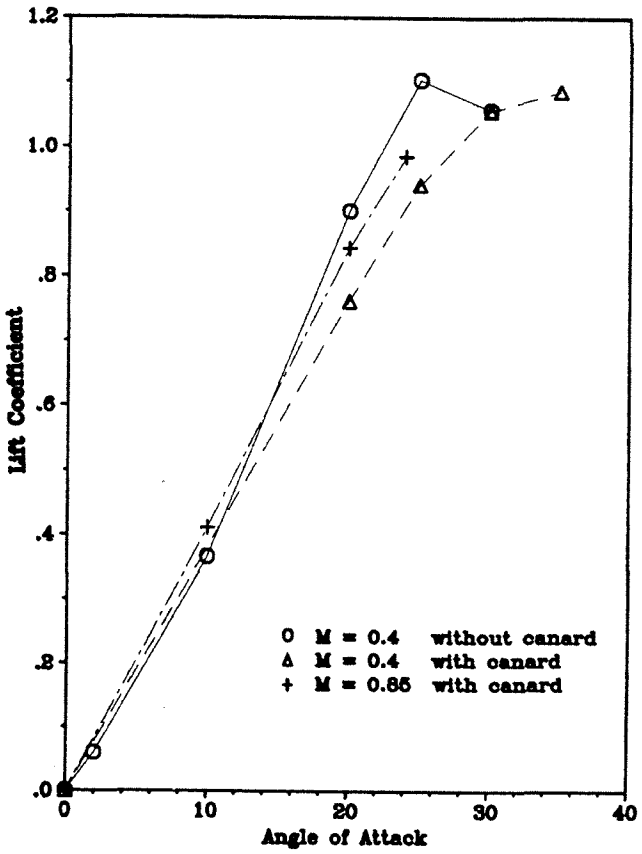

Fig. 4 Influence of angle of attack on lift.

Quantitative comparisons of c_p distributions and c_L values are difficult to perform for the two configurations due to differences in the meshes. Kumar and Das [30] have observed that the determination of total lift is strongly dependent on the mesh. It was not possible in this study to refine the mesh until a definitive value for c_L was obtained. Furthermore, the calculations for the delta wing alone were performed on the O-O mesh used in [30], whereas the canard-delta configuration was calculated on the H-H mesh described above. One calculation of the the delta wing alone was performed on an H-H mesh generated analogously to the canard-delta mesh. This produced a slightly lower value of c_L, which indicates that the applied H-H mesh does not resolve the flow near the surface as well as the O-O mesh. Nonetheless, comparison of sectional c_p distribution confirms the observation [31] that the effect of the canard is to reduce lift production in the inner part of the wing. (Figure 5). The sharp suction peak at the leading edge of the wing is an artificial effect due to the treatment of the leading edge singularity.

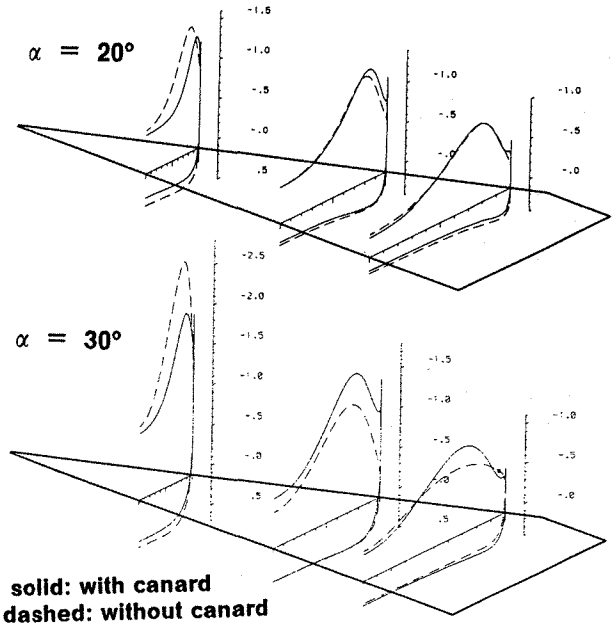

Fig. 5 Influence of canard on sectional c_p distribution.

Examination of simulated particle traces (Figure 6) indicate that the leading edge vortex from the canard rises and moves slightly inboard as it travels downstream. This is also indicated by examining crossflow velocities and total pressure losses in a plane perpendicular to the wing water line (Figures 7, 8).

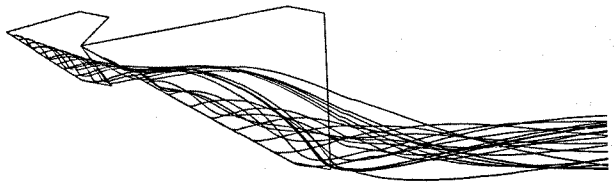

Fig. 6 Simulated particle traces for the canard-delta, M_∞ = 0.4, α = 20°.

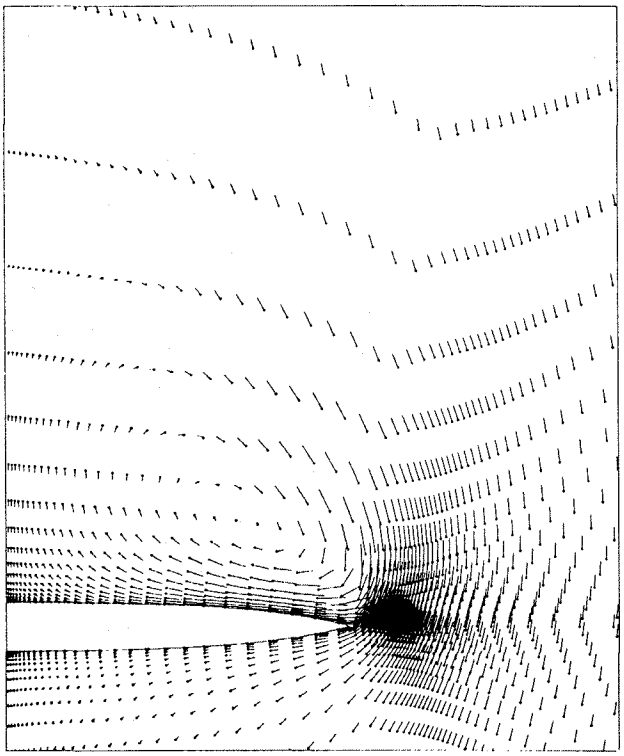

Fig. 7 Crossflow velocities, 60% root chord, M_∞= 0.4, α = 20°.

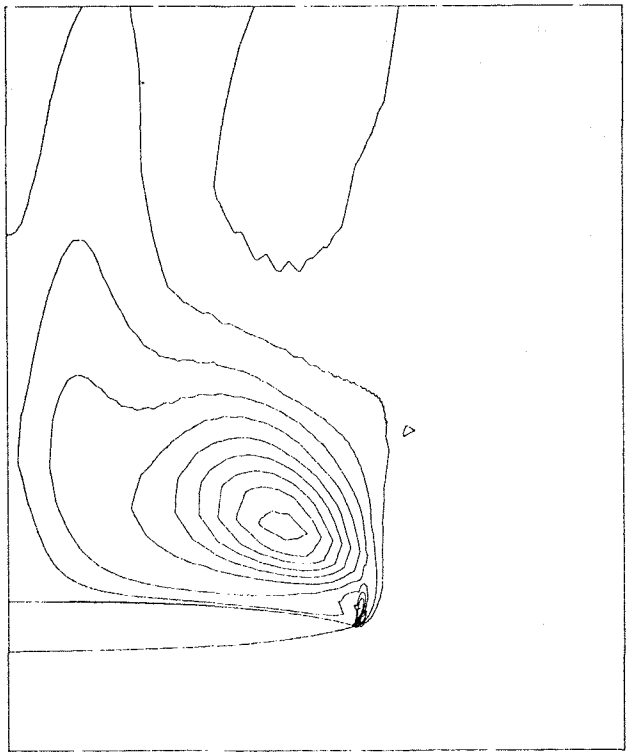

Fig. 8 Total pressure contours, 60% root chord, M_∞= 0.4, α = 20°.

Previous investigators [14] have determined that the loss of total pressure in the vortex core is well predicted by an inviscid code. Figure 9 illustrates the dependence of this value on angle of attack, Mach number, and also the influence of the canard. The total pressure loss increases with increasing angle of attack and Mach number, until bursting occurs. The influence of the canard effectively reduces the strength of the vortex and hence the total pressure loss.

Comments on the Simulation

Although the results of the computations are satisfactory, there remain a few points which require further investigation. The handling of the sharp H-grid singularities at the leading and trailing edges seems to introduce a very localized disturbance which did not occur in investigations for rounded edges. This is certainly an effect of the dissipation, as convective fluxes are correctly treated. The tiny cells at the apex singularity require very small timesteps for stability, and thus converge very slowly. They are necessary, however, if the leading edge is not to be on a block boundary or at a discontinuity in slope of the grid. Furthermore, computational effort could have been saved by using a C-grid structure at the wing trailing edge and the canard leading edge. This probably would have had little effect on the results. Lastly, the treatment of the tip edges in the canard-wing was very coarse and could be modelled more accurately.

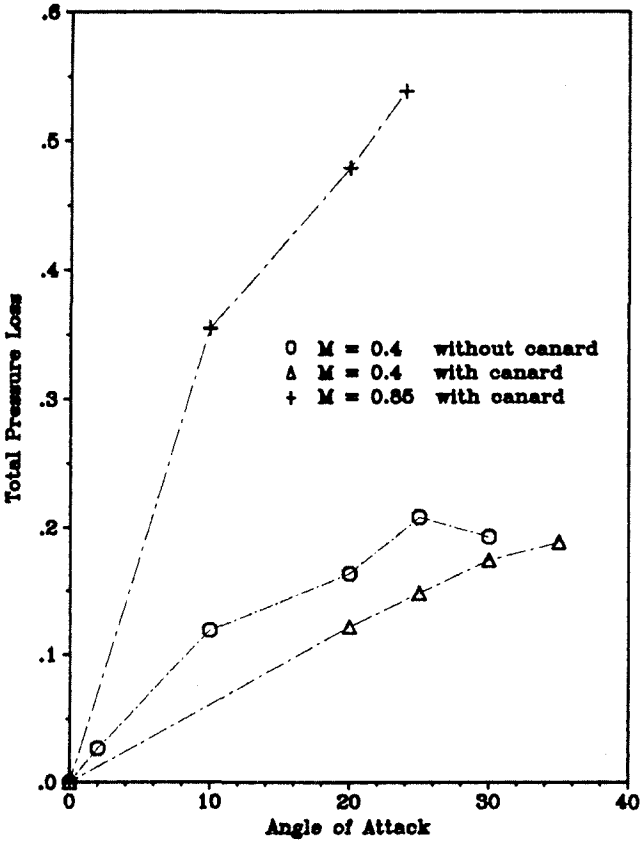

Fig. 9 Maximum total pressure loss vs. α, 80% root chord.

5. Analysis of the Vortical Flow Fields Around a Delta Wing Moving in an Inviscid Medium

An inclined surface moving through a medium at rest gives rise to a dipole distribution, which occurs due to the downward momentum imparted to the particles of the medium. The resulting flow picture resembles that of an electromagnetic field with flux lines going round the edges of the moving surface. The surface distribution of dipoles of varying strength can be represented as equivalent bound vortices on the wing. The interrelations between dipole strength, bound vorticity and the imparted downward momentum to the medium have been elucidated in [32].

The nature of the bound vortices on the wing surface and their changes with incidence

The flow around a delta wing with rolled up vortices has been calculated and the flow vectors on the wing surface used to determine the bound vortex lines. These are shown in Fig. 10 for $\alpha = 10°$ and $\alpha = 20°$ at a Mach number of 0.85. Due to the spiraling flow around the leading edges the bound vortices of a delta wing become highly curved and hence they differ widely from those of a high aspect ratio straight or swept wing.

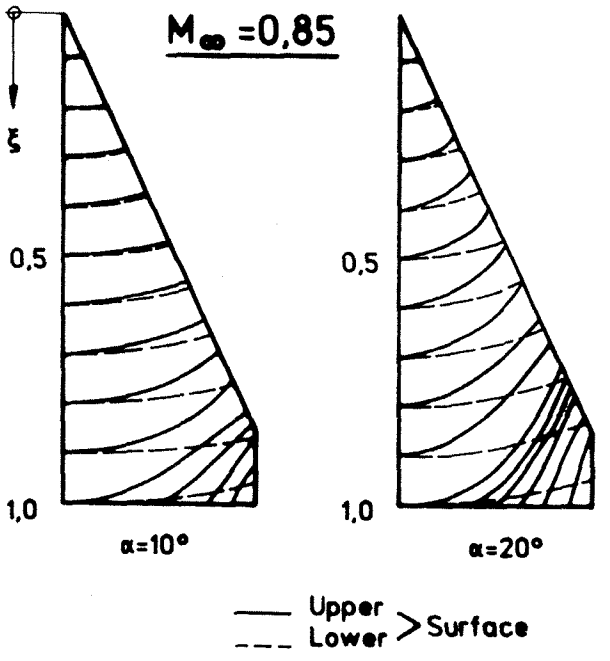

Fig. 10 Shapes of the bound vortex lines on the surface of an inclined delta wing moving in an inviscid medium.

At small angles of incidence ($\alpha < 10°$) the bound vortices on the upper and lower surfaces of the wing have almost identical shapes in the forward part of the wing, as predicted by linearized theory [4]. However at higher incidence, with increasing strength of the spiraling flow on the upper surface, the bound vortices on the two surfaces differ more and more from each other. The bound vortices become highly curved with increasing angles of incidence and some of them terminate at the trailing edge and leave the surface to continue as free vortices in the downstream flow.

It is quite evident that in the case of back flows at the rear part of the wing the bound vortices can curve around and terminate with both ends leaving the leading edge. A numerical field solution of this type can only be expected if Navier-Stokes equations are applied.

The vorticity in the flow field and the resulting total pressure losses

The bound vortices on the upper and lower surfaces of a delta wing will usually leave from the leading edge and take up spiraling motion in the flow field as free vortices. The strength of the vorticity shed from the leading edges can be determined from the surface vorticity of the wing. Using the momentum equation, denoted as the classical Euler equation in fluid mechanics, one can calculate the pressure field which creates the vortex structure and also the total pressure losses in the rolled up vortices inside the spiraling

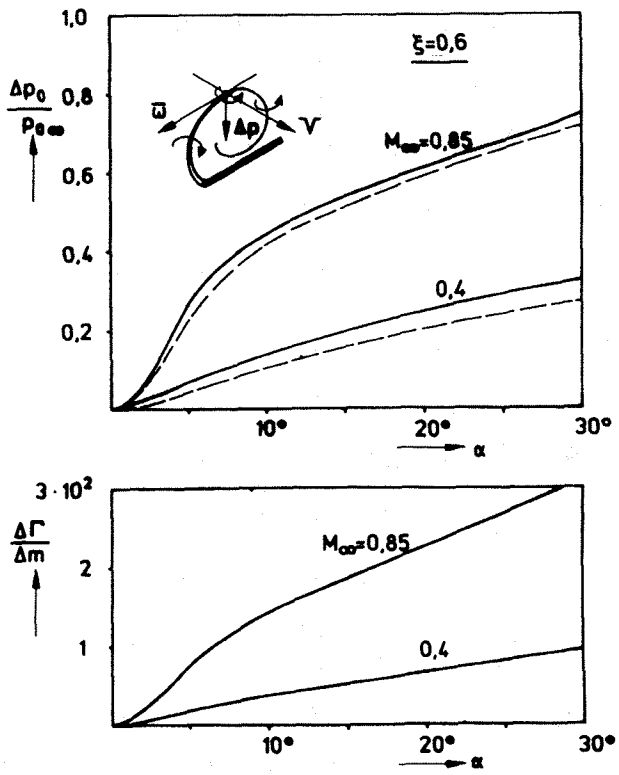

Fig. 11 Vortex shedding in the spiraling flow at the leading edges of a delta wing and the total pressure losses arising in the inviscid medium.

flow. The interrelations of surface vorticity at the leading edges, the pressure field and the total pressure losses in the vortex core are given in Fig. 11. The pressure gradient and the vorticity in the flow are related to the change in total pressure Δp_o through the second law of thermodynamics. The total pressure loss increases rapidly with the increase in incidence angle and the onflow Mach number.

The change of the flow field structure at higher incidence causing vortex break down

The nature of vortex roll-up around the leading edges of a delta wing is shown in Fig. 12 for $\alpha = 20°$ and $\alpha = 24°$ at an onflow Mach number of 0.85. While a typical coiling of the rolled-up vortices takes place at $\alpha = 20°$, the presence of high radial velocities in the region of the vortex sheet is clearly indicated in the case of $\alpha = 24°$. Thus for $\alpha > 24°$ no high surface velocity due to the spiraling vortex flow can come into being in the region concerned and this initiates a fall of the vortex lift.

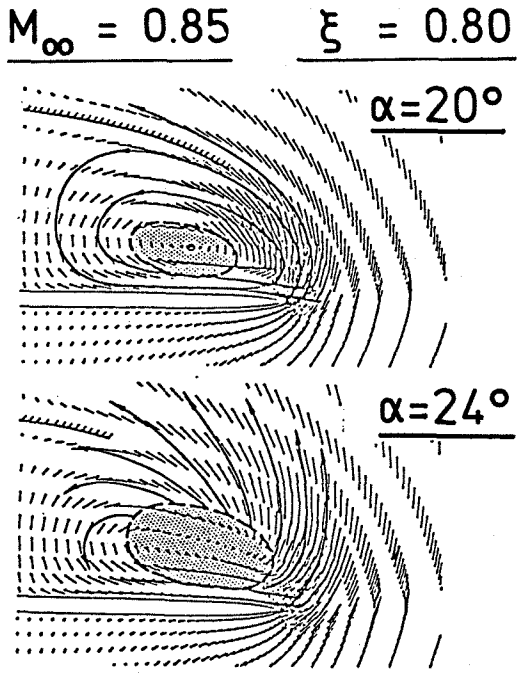

Fig. 12 Spiraling flow with vorticity arising on the lee side of an inclined delta wing moving through an inviscid medium.

The sudden origin of high radial velocities in the flow field can be attributed to counter-rotating vortices in the spiraling flow. This can be seen by analogy in the case of the electromagnetic flux lines generated by co-rotating and counter-rotating currents in a pair of coils. It is evident from Fig. 13 that in the counter-rotating flow case very intensive radial flux and high back flux come into being, thus totally destroying the normal field structure which prevails at moderate incidence.

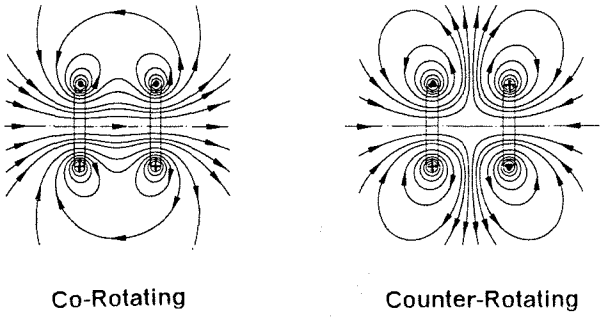

Fig. 13 Electromagnetic field lines around a series of ring coils with co-rotating and counter-rotating flow of currents.

In the case of the delta wing, the counter-rotating vorticity lines can come close together in two different ways when the Euler equations are solved and in three different ways when the Navier-Stokes equations are applied, in which case back flows and turning of the bound vortices on the wing surface can be expected. The three cases are illustrated in Fig. 14 with a and b arising from solution of the inviscid equations and a, b and c from the numerical method using Navier-Stokes equations. These types of encoun-

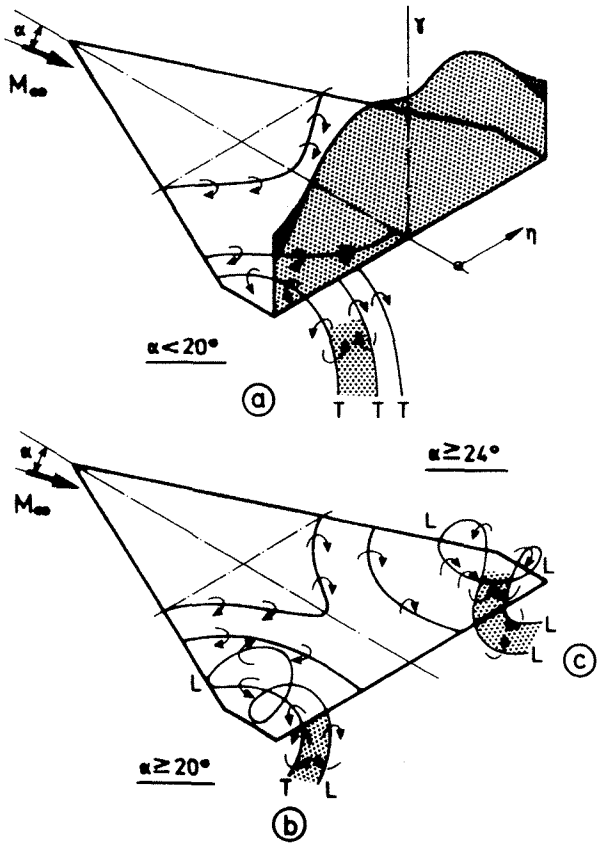

Fig. 14 Types of counter rotating vortices shed from delta wings causing vortex break down.

ters of vortex lines with counter- rotating vorticity are clearly observed both in numerical and experimental results.

6. Conclusions

The flowfield of a delta wing with canard has been simulated using the Euler equations. The H-H topology of the mesh enables uniform handling of leading and trailing edges. Comparison with calculations of the wing alone indicate that the influence of the canard leading edge vortex is to stabilize and reduce the strength of the wing leading edge vortex.

The interrelations between dipole distribution on the wing surface, the bound vorticity arising therefrom and the vortex shedding from the leading edges provide the necessary data for determing the total pressure loss in the rolled up vortices. The vortex breakdown phenomena can be directly attributed to the coiling up of counter-rotating vortices in the flow field, as they lie close to one another. The high radial velocities arising therefrom cause a marked swelling of the rolled up vortex sheet and destroy the spiraling structure of the flow.

Further research needs to be performed over a greater range of Mach numbers and angles of attack. Comparisons of canard on/canard off calculations would be better on meshes which are the same in both cases in the region of the main wing.

7. Acknowledgements

During the analysis of the flowfields some detailed and systematic parameter studies as well as a large number of plot programs have been necessary. The authors are indebted to J.M. Longo for providing active support and useful techniques in carrying out some of the evaluations of the results, and to N. Kroll for performing the calculations of the wing alone.

8. References

[1] Roy, M.: Remarques sur l'écoulement tourbillonnaire autour des ailes fleche. Z. angew. Math. Phys. 9b (1958), pp. 554-569. See also Sur la théorie de l'aile en delta. Tourbillons d'apex et nappes en cornet. La Recherche Aéronautique, No. 56 (1957), pp. 3-12.

[2] Legendre, R.: Nappes en cornet aux bords d'attaque d'une aile en delta. La Recherche Aéronautique, No. 70 (1959), pp. 3-10.

[3] Mangler, K.W.; Smith, J.H.B.: A theory of the flow past a slender delta wing with leading-edge separation. Proc. Roy. Soc. London (A) 251 (1959), S. 200-217: See also RAE TN 2593 (1957).

[4] Smith, J.H.B.: Improved Calculations of Leading Edge Separation from Slender, Thin Delta Wings. Proc. Roy. Soc., London, Series A 306 (1968). RAE Tech. Report No. 66070 (1966).

[5] Rehbach, C.: Calcul instationaire de nappes tourbillonnaires émises par des surface portantes fortment inclinées. Rech. Aerosp., No. 1978-83.

[6] Belotserkovskii, S.M.: Nonstationary nonlinear theory of a thin wing of arbitrary planform. Izv. Akad. Nouk SSSR, Mekh. Zhidk Gaza 4: 100-8, Fluid Dyn. 9 (4), (1974) pp. 583-89.

[7] Weber, J.A., Brune, G.W., Johnson, F.T., Lu, P., Rubbert, P.E.: A three-dimensional solution of flows over wings with leading-edge vortex separation. AIAA Paper 75-866, Hartford, Conn. (1975).

[8] Kandill, O.A., Chuang, A., Chu, L.C.: Finite-Volume and Integral Equation Techniques for Transonic and Supersonic Vortex Dominated Flows. ICAS Proceedings, 1986, pp. 629-640.

[9] Rizzi, A., Eriksson, L.E., Schmidt, W., Hitzel, S.M.: Simulating Vortex Flows Around Wings. AGARD CP No. 342, April 1983, pp. 21.1-21.14.

[10] Fujii, K., Kutler, P.: Numerical Simulation of the Leading-Edge. Separation Vortex for a Wing and Strake-Wing configuration. AIAA Paper 83-1908-CP, 6th Computational Fluid Dynamics Conference, Danvers, Massachusetts, July 13-15, 1983.

[11] Hitzel, S.M., Schmidt, W.: Slender Wings with Leading-Edge Vortex Separation: A Challenge for Panel Methods and Euler Solvers. AIAA Journal of Aircraft, Vol. 21, No. 10, October 1984, pp. 751-759.

[12] Murman, E.M., Rizzi, A.: Application of Euler Equations to Sharp Edge Delta Wings With Leading Edge Vortices. AGARD Symposium on Application of Computational Fluid Dynamics in Aeronautics, Aix-en- Provence, France, April 7-10, 1986.

[13] Raj, P., Sikora, J.S., Keen, J.M.: Free Vortex Flow Simulation Using A Three-Dimensional Euler Aerodynamic Method. ICAS Proceedings, Vol. 1, 1986, pp. 604-617.

[14] Rizetta, D.P., Shang, J.S.: Numerical Simulation of Leading Edge Vortex Flows. AIAA Journal, Vol. 24, No. 2, February 1986, pp. 237-245.

[15] Thomas, J.L., Newsome, R.W.: Navier-Stokes Computations of Lee-Side Flows over Delta Wings. AIAA Paper 86-1049, May 1986.

[16] Werlé, H.: Sur l'éclatement des tourbillons d'apex d'une aile delta aux faibles vitesses. La Recherche Aéronautique, N0. 74 (1960), pp. 23-30.

[17] Squire, H.B.: Analysis of the "Vortex breakdown" phenomenon, Part I. Imperial College of Science and Technology, University of London, Aeron. Dept. Rep. 102 (1960). In: M. Schäfer (Editor): Miszellaneen der Angewandten Mechanik (Festschrift Walter Tollmien). Akademie-Verlag, Berlin 1962, pp. 306-312.

[18] Elle, B.J., Jones, J.P.: A note on the velocity distribution on the surface of slender delta wings with leading-edge separation. J.Roy. Aeron.Soc.65 (1961), pp. 195-198.

[19] Hummel, D.: On the vortex formation over a slender wing at large angle of incidence. AGARD-Symposium "High Angle of Attack Aerodynamics", Sandfjord, Norway, Oct. (1978). AGARD-CP-247, pp. 15-1 to 15-17.

[20] Bütefisch, K.A.: Flow Field Study on a 65° Delta Wing. International Vortex Flow Experiment on Euler Code Validation, Symposium FFA, Stockholm, Oct. 1.-3. 1986.

[21] Boersen, S.J., de Brin, A.C., Hoeijmakers, H.W.M., Elsenaar, A.: Test of the AFWAL 65° Delta Wing at NLR. A Study of Vortex Development between Mach = 0.4 and 4. International Vortex Flow Experiment on Euler Code Validation. Symposium FFA, Stockholm, Oct. 1.-3. 1986.

[22] Hirdes, R.H.C.M.: International Vortex Flow Experiment - Test Report of Wind Tunnel Measurements on the 65° Wing in the NLR High Speed Wind Tunnel HST. NLR TR 85046L,May 1985.

[23] Hartmann, K.: International Transonic Vortex Flow Experiment, Plots of Pressure Measurements. DFVLR IB 222-86A23 (1986). Plots of Force Measurements. DFVLR IB 222-85A36 (1986).

[24] Jameson, A., Schmidt, W., Turkel, E.: Numerical Solution of the Euler Equations by Finite Volume Methods Using Runge Kutta Time Stepping Schemes. AIAA-Paper, 81-1259 (1981).

[25] Radespiel, R., Kroll, N.: Progress in the Development of an Efficient Finite Volume Code for the Three-Dimensional Euler Equations. DFVLR-FB 85/31, 1985.

[26] Rossow, C.C.: Berechnung von Strömungsfeldern durch Lösung der Euler-Gleichungen mit einer erweiterten Finite-Volumen Diskretisierungsmethode. Dissertation der TU-Braunschweig, 1988. (To be published as DFVLR-FB).

[27] Rossow, C.; Kroll, N.; Scherr, S.; Radespiel, R.: Investigation of the accuracy of Finite Volume Methods for 2- and 3-Dimensional Flows. Proceedings of AGARD Conference on Validation of Computational Fluid Dynamics, Lisbon, AGARD-CPP-437, Paper P-17 (1988).

[28] Hall, M.G.: Cell Vertex Multigrid Scheme for Solution of the Euler Equations. Proceedings of the Conference on Numerical Methods for Fluid Dynamics, Reading, U.K. (1985).

[29] Kroll, N, Jain, R.K.: Solution of Two-Dimensional Euler Equations - Experience with a Finite Volume Code. DFVLR-FB 87/41, 1987.

[30] Kumar, A., Das, A.: Computation of Vortex Flow on a Delta Wing at Transonic Speed. IUTAM Symposium Transsonicum III (1988).

[31] Eriksson, L., Rizzi, A.: Computation of Vortex Flow around a Canard-Delta Combination. Proceedings of the 5th GAMM Conference on Numerical Methods in Fluid Mechanics, (1983).

[32] Das, A.: On the Kutta Condition for Lifting Aerofoils and Wings. DFVLR FB 87-40, 1987.